A Single-Phase Grid-tied PV based Trans-Z-Source Inverter Utilizing LCL filter and Grid Side Current Active Damping

Majid Hosseinpour[1*] and Navid Rasekh[1]

[1]*Department of Electrical and Computer Engineering, University of Mohaghegh Ardabili, Ardabil, Iran*
**Corresponding author: hoseinpour.majid@uma.ac.ir*

Manuscript received 25 January, 2019; revised 25 February, 2018; accepted 5 March, 2019. Paper no. JEMT-1901-1150.

As grid-connected Photovoltaic (PV) based inverters are being used more, these systems play a more important role in the electricity generation by distributed power generators. Power injection to the grid needs to meet predefined standards. In this work, a PV based inverter consists of a Trans-Z-Source network performing as DC-DC power conversion level, is connected to the grid through a LCL filter. The connection through an LCL filter offers certain advantages, but it also brings the disadvantage of having a resonance frequency. A systematic mathematical design procedure for PR controller parameters along with active damping factor is presented and the overall control system leads to a considerably low value of grid current THD. Meanwhile the Maximum Power Point Tracking (MPPT) of the PV arrays is obtained by a modified INC method. Simulations in various conditions are carried out in MATLAB/Simulink environment and results depict suitable performance of the system with designed parameters.

Keywords: *Trans-Z-Source Inverter, PV systems, PR controller, LCL filter, Active Damping*

http://dx.doi.org/10.22109/jemt.2019.169380.1150

Nomenclature

T	switching period
T_{nsh}	none-shoot-through duration
T_{sh}	shoot-through duration
D_{sh}	shoot-through duty cycle
B	boost factor
n	Transformer turn ratio
L_1	Inverter side filter inductance
C	filter capacitance
L_2	grid side filter inductance
U_{sc}	output of the MPPT block
K_P	proportional gain
K_r	resonance gain
ω_{PRc}	bandwidth around the resonance frequency
ω_1	fundamental frequency
K_{AD}	active damping factor
φ	angle between currents of inverter side and grid side inductances
V_g	RMS value of the grid voltage
I_{ref}	RMS value of the reference current
T_{f1}	magnitude of the open loop Transfer function at fundamental frequency
PM	desired phase margin for the system

1. Introduction

Increasing tendency toward generation of electricity using renewable energy resources like solar power and wind power has motivated scientists and researchers to study Distributed Power Generation (DPG) and develop it as an alternative for fossil based energy resources. As the cost of solar panels are still high, it is important to make more power use of these panels by improving its power conversion efficiency. Due to nonlinear V-I characteristic in each weather condition, photovoltaic (PV) array has an individual maximum output power operating point. Various techniques have been proposed in the literature to track the Maximum Power Point (MPP). The two frequently used maximum power point tracking (MPPT) methods are Perturb-and-Observe (P&O) and Incremental Inductance (INC) [1].

In a grid connected PV system, the output voltage of the PV array is connected to the AC grid through an inverter. In traditional Voltage Source Inverters (VSI) the DC voltage is converted to ac voltage and the output of the VSI is less than input DC voltage. This leads to additional DC-DC boost converter in case voltage boost is required. However both switches of each phase leg can't be switched on simultaneously, because short circuit destroys the device[2]. The disadvantages of traditional VSI are eliminated by emerging of Z-Source inverters [3] in which an additional shoot-through state along with non-shoot-through state and active state are applied using different modulation techniques [4, 5].

Z-Source inverters cannot operate in bidirectional power flow mode and the voltage gain is obtained in large shoot-through time.

These issues and limits led to introduction of a Transformer based inverter structure called Tran-Z-Source [6]. In this inverter topology, higher boost gain is achievable with the same shoot-through duty cycle and modulation index compared with Z-Source inverter. There have been other modified and developed structures based on Z-Source inverter and its operation mode in shoot-through state in the literature like Y-Source Impedance Network [7], quasi Y-Source boost DC-DC converter [8], quasi impedance source [9] and a high performance quasi Z-Source converter for photovoltaic applications has been proposed in [10]. If the proposed structures are compared in terms of efficiency, cost and volume, Trans-Z-Source inverter functions quite well in most of the considered terms [6, 11] . Therefore, this structure is chosen for DC-DC conversion level along with an H-Bridge inverter in this paper.

DPG systems need power electronics converter as an interface between the energy source and the grid/consumer. The output of the Trans-Z-Source converter and H-Bridge inverter consists of three levels, therefore, to meet harmonic standards like IEEE std 1547 [12] an output filter is needed. Among different filter types, LCL filter has superior performance at high frequencies in comparison with L an LC filters and it is not as complicated as high order filters [13]. LCL filter parameter design is another issue that effects on output power quality directly. In [14] and the recent work in [15] the parameter design of LCL filter design is thoroughly discussed considering grid standards for the quality of injected power.

One of the troubling constraints of LCL filter is the resonance phenomenon, which can cause stability problems. So damping is required to suppress filter resonance. Passive damping methods require resistance connection either in parallel or series with filter capacitor, but this resistance leads to power loss, which is not desirable. Active damping methods use control approaches to achieve the same goal. Compared with passive damping, active damping methods have attacked more attention due to their flexibility and lower damping power losses. However, the control complexity and the cost of the sensors will be increased [16].

The two main types of AD can be categorized to single loop and multi loop methods. Multi loop AD methods include a virtual resistor [17]-[19], capacitor current feedback [20]-[25], capacitor voltage feedback [26]-[29], and LC-trap voltage feedback [30]. One of the most popular active damping methods is using the capacitor current feedback which results in suitable stability characteristic [31]. Similar to the capacitor current feedback active damping method, the derivative feedback of the capacitor voltage can also induce effective active damping [26]-[28]. Using an LLCL filter, a LC-trap voltage feedback method is introduced in [30] and indicated that the introduced method had a wider damping region in comparison with the capacitor current feedback active damping. However, as the grid voltage may experience a sudden and large change, it is difficult to choose a suitable feedback coefficient to ensure a satisfactory damping effect under different grid voltage conditions [31].

The main aim of DPGs is to provide suitable power quality to the grid, so choosing appropriate controller to control current injected to the grid be of high importance to deal with resonance frequency caused by LCL filter.

Proportional Resonance (PR) controller can tackle this issue by providing infinite gain at the intended frequency and it can track sinusoidal waveform reference with zero steady state error [32]. A grid tied inverter with LCL type inverter using PI and PR controllers as the injected current regulator and considering active damping of filter capacitance current has been proposed in [23] in which a systematic design procedure is proposed for tuning the PI controller considering AD but the design procedure is not elaborate for PR controller and a step by step design procedure for PR compensator along with capacitor current active damping is missing. A capacitor-current feedback active damping method is proposed in [33] to increase the system critical frequency greatly and to obtain a wider damping region for all possible LCL resonances. Despite the ability in damping region expansion, this method is not systematic and step-by-step procedure. A systematic method considering active damping and PR controller has been proposed in [34] to design control parameters. The feedforward gain of the grid voltage effect point and its regarding gain is vague as the PR controller cannot track voltage and current error in the same point. In this paper, a systematic design procedure is presented to design PR controllers' parameters as well as filter capacitor current feedback coefficient. Complexity and ambiguity of mentioned previous works has been tried to be revised.

In the area of grid connected PV systems, a two level sensorless grid tied system with constant power generation control is proposed in [35] which applies a LCL filter. A LCL grid connected VSI applying inverter side current control with generalized predictive control is also proposed in [36]. A grid tied single-phase power conditioning system for Trans-Z-Source based inverter is proposed in [11], which has applied a L filter controlling the current injection to the grid by a PR controller to meet grid codes. The grid current THD in [11] less than 3% and as such systems are usually used in week grids, they're highly exposed to grid voltage fluctuations which leads to varying grid side inductance, the quality of the injected current to the grid might not be sufficient.

Considering the advantages and disadvantages of the previous works, in this paper a single-phase LCL-type PV based Trans-Z-Source inverter applying grid current control along with active damping has been proposed. The main novelty of this paper is introducing a feasible and systematic procedure to design proportional resonant controllers' parameters elaborately as well as filter capacitor current feedback coefficient. The designed control coefficients to PV based power conditioning system will result considerable THD reduction of the injected current to grid.

The rest of this paper is organized as follows. In section 2, the principles of Trans-Z-Source inverter is discussed. The power injection control of the grid-connected system is presented in section 3. In section 4, the control scheme and step-by-step design procedure of the controllers are investigated. Simulation results are given in section 5 and a comparison of obtained results with other researches is presented in section 6. Finally, section 7 concludes this paper.

2. Principles of Trans-Z-Source Inverter Performance

There have been several Transformer based topologies which are derived from different topologies i.e. voltage fed quasi Z-Source, current fed quasi Z-Source [37, 38], voltage fed Z-Source and current fed Z-Source [3, 38]. In this paper voltage-fed Trans-Z-Source [6] is considered to function as DC-DC converter.

Trans-Z-Source inverter is capable of operating in both shoot-through state and non-shoot-through state. In the shoot-through state, either the upper and lower switches of each leg or two legs (T1&T2 or T3&T4 or all the switches) are on to produce the desired ac voltage. Table 1 summarizes switching modes containing two active states, two zero output voltage states and five different shoot-through modes.

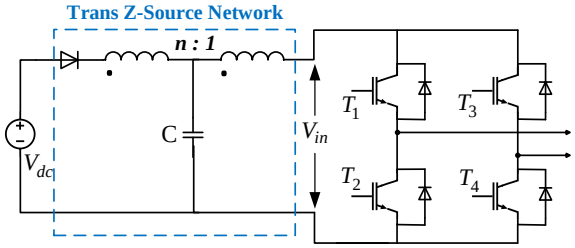

Fig. 1. A single-phase Trans Z-Source based inverter

Table 1. Switching modes in a single phase Trans-Z-Source inverter

Switching modes	T_1	T_2	T_3	T_4
Shoot-through	1	1	0	0
Shoot-through	1	1	1	0
Shoot-through	0	1	1	1
Shoot-through	1	0	1	1
Shoot-through	1	1	1	1
Active	1	0	0	1
Active	0	1	1	0
Zero	0	1	0	1
Zero	1	0	1	1

Voltage boost in Trans-Z-Source converter occurs at shoot-through mode. If T, T_{nsh} and T_{sh} represent switching period, none-shoot-through duration and shoot-through duration, respectively, voltage boost happens in T_{sh}. Consequently shoot-through duty cycle is the ratio of T_{sh} and T ($D_{sh} = T_{sh} / T$). The relationship between input voltage of the H-Bridge inverter (V_{in}) and input DC voltage (V_{dc}) is $V_{in}=BV_{dc}$. B is the boost factor which is derived from Trans-Z-Source equations considering the average voltage of both inductors to be zero over one switching period in the steady state. Thus, the capacitor voltage will be [6]:

$$V_{C_{TR}} = \frac{1-D_{sh}}{1-(1+n)D_{sh}} V_{dc} \quad \textbf{(1)}$$

Considering governing equations of Trans-Z-Source inverter in both shoot-through and none-shoot-through modes, the boost factor is calculated as following [6]:

$$B = \frac{1}{1-(1+n)D_{sh}} \quad \textbf{(2)}$$

As depicted in (2) B is dependent on shoot-through duty, cycle and Transformer turn ratio. The more each of them be, the more gain is expected at the output.

3. Power injection control of the grid connected system

As shown in Fig. 1 the system is composed of a voltage boost level, which is DC-DC Trans-Z-Source network and the boosted voltage is fed to an H-Bridge. To ensure power injection to the grid with good quality, a control system is needed to obtain MPP and inject power with unity power factor along with controlling grid current THD according to grid standards. MPPT plays an important role in the control system. In the next subsection, the applied MPPT method in this system is discussed.

3.1. MPPT Technique

Because of the non-linear output characteristics of the PV array, the tracking of the MPP at various environmental conditions can sometimes be a challenging task. Various MPPT methods have been proposed in the literature. Among all, the Perturbation and Observation (P&O) [39] and Incremental Conductance (INC) [40] are the most frequent techniques that have been applied in different PV systems.

The extraction of maximum possible electric energy from photovoltaic arrays is the common and final purpose of all MPPT control methods. As shown in Fig. 2, the employed MPPT algorithm is based on the INC method in which the inputs are the measured PV voltage and current values. A Low Pass Filter (LPF) is applied on the measured PV voltage and current to have a better sample. A

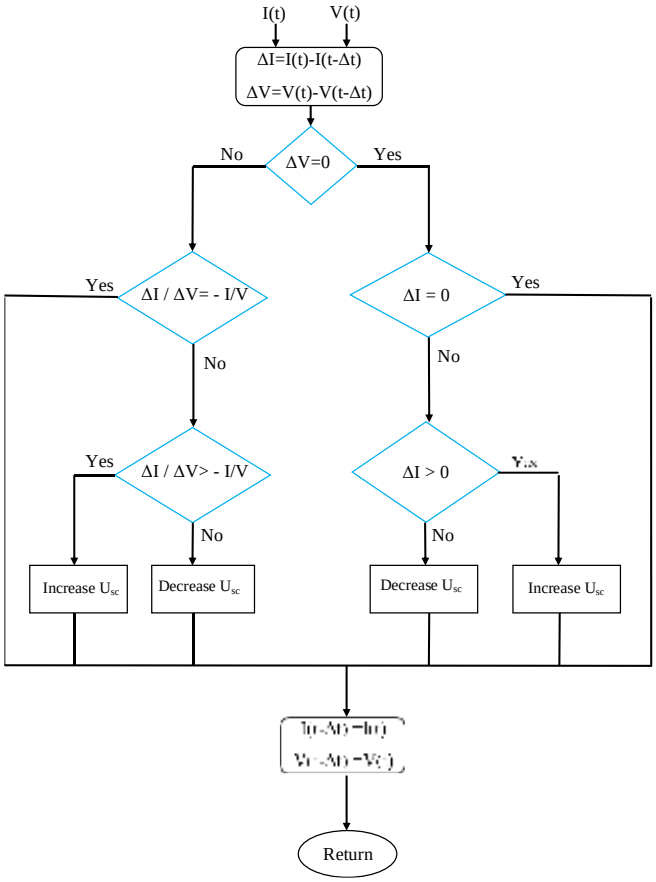

Fig. 2. Modified MPPT algorithm

variable value of D_{sh} is determined by the MPPT algorithm and the output of the MPPT is $U_{sc} = 1 - D_{sc}$ which controls the shoot-through mode of the switching modulation.

Simple boost method is used as the modulation technique [3], in which the control signal is V_{ref}^* that will be discussed in the next subsection and a direct line that is the output of the MPPT block (U_{sc}).

3.2. Injected current to the grid control

A PV system is connected to the grid to deliver power according to the grid standards. Control of the power flow to the grid is an issue that should be addressed.

Voltage of DC-link capacitor is a good criterion to indicate the power flow. When this voltage exceeds its reference value, the control system should lower the shoot-through duty cycle and in case the reference voltage has higher value, the shoot-though duty cycle should be increased by the control system so that the stability of the system be ensured.

As shown in Fig. 3, the voltage of Trans-Z-Source network capacitor is sampled and compared with its reference value. Then the error signal is controlled by a PI controller to produce the reference amplitude of the reference current. To achieve unity power injection, a Phase Locked Loop (PLL) block derives the phase of the grid voltage and multiplying it to the value of the output of the PI controller, and it also produces the reference current (i_g^*) for injected grid current control. By subtracting the grid sampled current from i_g^* the error signal is applied to a Proportional Resonance (PR) controller. To ensure good quality power injection an active damping method is also employed. The parameter design of the active damping factor and PR controller is discussed in the next section.

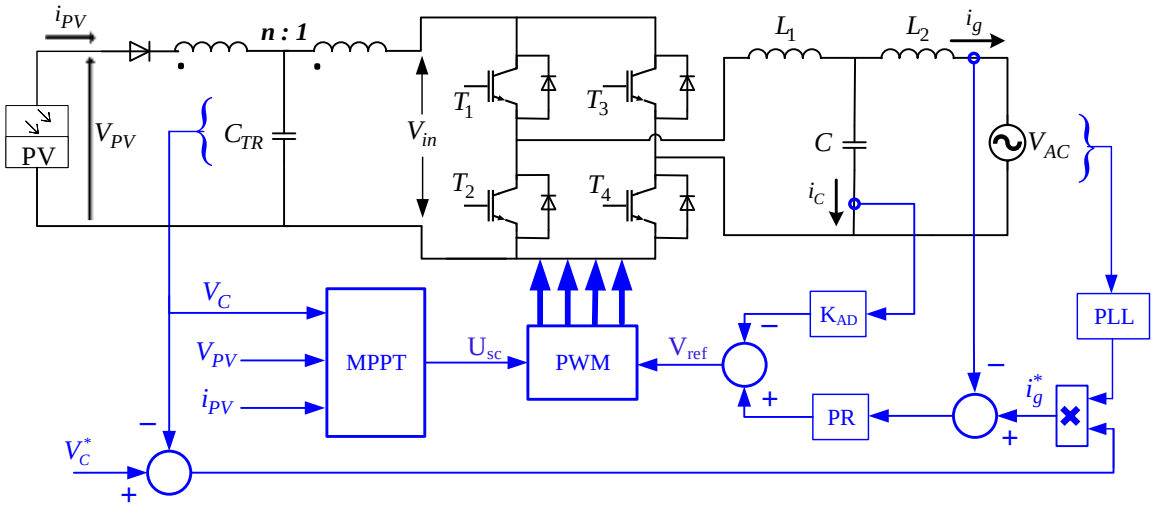

Fig. 3. Control scheme of a single-phase grid connected Trans-Z-Source inverter PV system

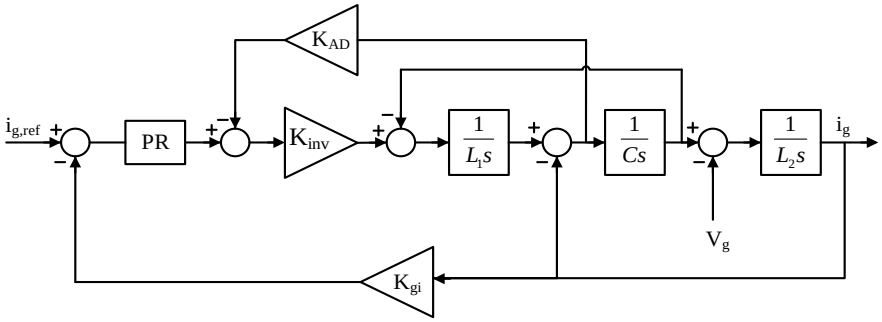

Fig. 4. Control block diagram of PR controller and active damping

Writing Kirchhoff's laws for the system results in (3).

$$\begin{cases} L_1 \dfrac{di_1}{dt} = u_i - u_c \\ L_2 \dfrac{di_g}{dt} = u_c - u_g \\ C \dfrac{du_c}{dt} = i_c \\ i_1 = i_g + i_c \end{cases} \quad (3)$$

As resistances of filter inductances and capacitor are neglected through design procedure, they are not shown in Fig. 3. The equivalent block diagram of the system is shown in Fig. 4. As can be seen, the actual injected current to the grid is differentiated from the reference current, which is calculated by the upstream power control. The error goes through a PR controller to create reference voltages for the inverter.

To compensate filter resonance peak, a feedback of filter capacitor current is added to these references. Design of controller parameters and capacitor current feedback coefficient is discussed in the following section.

4. Design of PR Controller and Active Damping

4.1. Control Scheme Modelling

The transfer function of a non-ideal PR controller is shown by (7) in which K_P, K_r are proportional gain and resonance gain and ω_{PRc}, ω_1 represent bandwidth around the resonance frequency and the fundamental frequency, respectively. The non-ideal PR controller's sensitivity to resonance frequency drift is less than the ideal PR controller. Ideal PR controller which is shown in (6) is also not realizable due to component tolerances in analog systems and finite precision in digital system [32,41]. The diagram shown in Fig. 4 can be simplified to the one in Fig. 5 in which $G_1(s)$, $G_2(s)$ and $G_{PR}(s)$ are:

$$G_1(s) = \frac{K_{inv} G_{PR}(s)}{CL_1 s^2 + K_{inv} K_{AD} Cs + 1} \quad (4)$$

$$G_2(s) = \frac{CL_1 s^2 + K_{inv} K_{AD} Cs + 1}{L_1 L_2 Cs^3 + L_2 CK_{AD} K_{inv} s^2 + (L_1 + L_2)s} \quad (5)$$

$$G_{PR}(s) = K_P + \frac{2K_r s}{s^2 + \omega_1^2} \quad (6)$$

$$G_{PR}(s) = K_P + \frac{2K_r \omega_{PRc} s}{s^2 + 2\omega_{PRc} s + \omega_1^2} \quad (7)$$

K_{AD} is the active damping factor and $G_{PR}(s)$ is PR controller Transfer function. According to Fig. 5, the open loop Transfer function is calculated as following:

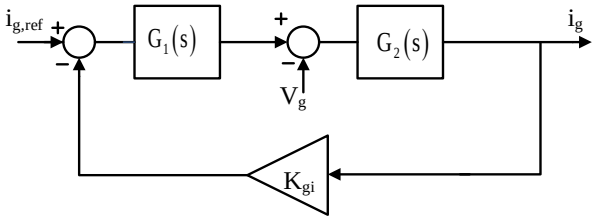

Fig. 5. Equivalent block diagram of control scheme

$$T(s)=\frac{K_{gi}K_{\mathrm{AD}}G_{\mathrm{PR}}(s)}{L_1L_2Cs^3+L_2CK_{\mathrm{AD}}K_{\mathrm{inv}}s^2+(L_1+L_2)s} \quad (8)$$

If the grid current be considered as the effects of reference current and grid voltage, it can be inferred that:

$$i_g(s)=i_{g1}(s)+i_{g2}(s) \quad (9)$$

Where

$$\begin{cases} i_{g1}(s)=\dfrac{1}{K_{gi}}\dfrac{T(s)}{1+T(s)}i_{ref}(s) \\ i_{g2}(s)=-\dfrac{G_2(s)}{1+T(s)}V_g(s) \end{cases} \quad (10)$$

According to Fig. 6 and considering φ as the angle between $i_{g1}(s)$ and $i_g(s)$:

$$\tan(\varphi)=\left|\frac{i_{g2}(s)}{i_{g1}(s)}\right|=\left|\frac{K_{gi}G_2(s)V_g(s)}{T(s)i_{ref}(s)}\right|_{s=j\omega_1}=\left|\frac{K_{gi}G_2(j\omega_1)}{T(j\omega_1)}\frac{V_g(j\omega_1)}{i_{ref}(j\omega_1)}\right| \quad (11)$$

By substituting $s=j\omega_1$ in $G_{PR}(s)$:

$$G_{PR}(j\omega_1)=K_P+\frac{2K_r\omega_{PRc}j\omega_1}{(j\omega_1)^2+2\omega_{PRc}j\omega_1+\omega_1^2}=K_P+K_r \quad (12)$$

The capacitor of LCL filter can be ignored since the LCL filter resonance frequency is much greater than the fundamental frequency [41]:

$$\begin{cases} C=0 \\ G_2(j\omega_1)=\dfrac{1}{(L_1+L_2)(j\omega_1)} \end{cases} \quad (13)$$

Thus, it can be deduced that:

$$\begin{cases} \tan(\varphi)=\left|\dfrac{K_{gi}}{T(j\omega_1)(L_1+L_2)(j\omega_1)}\right|\left|\dfrac{V_g(j\omega_1)}{i_{ref}(j\omega_1)}\right| \\ T(j\omega_1)=\dfrac{K_{gi}}{\tan(\varphi)(L_1+L_2)(\omega_1)}\cdot\dfrac{V_g}{I_{ref}} \end{cases} \quad (14)$$

V_g is the root mean square (RMS) value of the grid voltage and I_{ref} is the RMS value of the reference current. T_{f1} is considered as the magnitude of the open loop Transfer function at f_1 (fundamental frequency), in dB.

$$T_{f1}=20\log|T(j\omega_1)|=20\log\left(\frac{K_{gi}V_g}{\tan(\varphi)I_{ref}(L_1+L_2)(\omega_1)}\right) \quad (15)$$

According to Fig. 5 current error E_A can be calculated as following:

$$E_A=\frac{|K_{gi}i_g(j\omega_1)|-I_{ref}}{I_{ref}}=\frac{K_{gi}|i_{g1}(j\omega_1)/\cos\varphi|}{I_{ref}}-1 \quad (16)$$

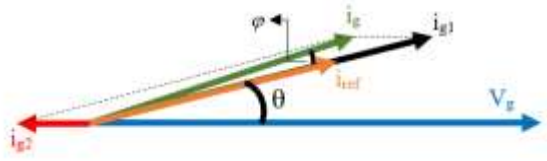

Fig. 6. Phasor diagram of the grid voltage and injected grid current

Substituting $i_{g1}(s)$ from (10) to (16), E_A can be expressed as:

$$E_A=\left|\frac{T(j\omega_1)}{1+T(j\omega_1)}\right|\frac{1}{\cos\varphi}-1 \quad (17)$$

If $T_{f1}\geq 40dB$ then $1+T(j\omega_1)\approx T(j\omega_1)$, so (14) can be rewritten:

$$E_A=\left|\frac{T(j\omega_1)}{1+T(j\omega_1)}\right|\frac{1}{\cos\varphi}-1\approx\frac{1}{\cos\varphi}-1 \quad (18)$$

According to (18) and Fig. 6, to achieve zero error $\cos\varphi=1$ which means. $\varphi=0^\circ$ .. As the phase of the reference current is defined by a phase locked loop (PLL) of the grid voltage, $i_{ref}(s)$ and $V_g(s)$ have the same phase ($\theta=0$).

4.2. Proportional – Resonant Controller

4.2.1 Proportional Gain (K_P)

The resonance frequency of LCL filter can be obtained by equation (19).

$$f_{res}=\frac{1}{2\pi}\sqrt{\frac{L_1+L_2}{L_1L_2C}} \quad (19)$$

The crossover frequency (f_c) value is usually chosen lower than switching frequency (f_{sw}) to prevent the effect of attenuating high frequency noise. Resonance frequency of the LCL filter is typically constrained in the range of $f_{sw}/4$ to $f_{sw}/2$ in order to suppress harmonics and function with a good dynamic. To fulfil appropriate design and suitable performance of the LCL-type grid connected Trans-Z-Source inverter, f_c is chosen a value lower than $f_{sw}/10$. Since f_c is about ten times smaller than f_{sw} and it is also smaller than resonance frequency of LCL filter, the impact of the capacitor can be overlooked [42], so the open loop Transfer function of the system can be derived as:

$$|T(s)|\approx\left|\frac{K_{gi}K_{\mathrm{inv}}G_{\mathrm{PR}}(s)}{(L_1+L_2)s}\right| \quad (20)$$

PR controller equation can be simplified since the cut-off frequency is greater than the fundamental frequency, therefore the resonance term of PR controller is ignored and (21) is concluded.

$$G_{PR}(j\omega_c)=K_P+K_r\approx K_P \quad (21)$$

The open loop Transfer function can be rewritten as follows:

$$|T(j\omega_c)|\approx\left|\frac{K_{gi}K_{\mathrm{inv}}K_P}{(L_1+L_2)j\omega_c}\right| \quad (22)$$

The amplitude of system frequency response is zero in cut-off frequency and it can be used to calculate proportional gain.

$$20\log\left|G(j2\pi f_c)\right| \approx 20\log\left|\frac{K_{gi}K_{inv}K_P}{(L_1+L_2)j\omega_c}\right| = 0 \quad \textbf{(23)}$$

$$K_P = \frac{2\pi f_c(L_1+L_2)}{K_{gi}K_{inv}} \quad \textbf{(24)}$$

4.2.2 Resonant Gain (K_r)

Considering PR controller Transfer function as (7), in cut off frequency ($f = f_1$) (7) can be rewritten as:

$$G_{PR}(j\omega_1) = K_P + \frac{2K_r\omega_{PRc}(j\omega_1)}{(j\omega_1)^2 + 2\omega_{PRc}(j\omega_1) + \omega_1^2} = K_P + K_r \quad \textbf{(25)}$$

According to (20) and (24) it is inferred that:

$$\left|T(s)\right|_{s=jw_1} \approx \left|\frac{K_{gi}K_{\text{inv}}(K_P+K_r)}{(L_1+L_2)(j\omega_1)}\right| \quad \textbf{(26)}$$

Considering (15) leads to (27) and (28)

$$\begin{cases} T_{f1} = 20\log\left|T(j\omega_1)\right| \\ T_{f1} = 20\log\left|\dfrac{K_{gi}K_{\text{inv}}(K_P+K_r)}{(L_1+L_2)(j\omega_1)}\right| \end{cases} \quad \textbf{(27)}$$

$$K_r = \frac{2\pi(L_1+L_2)}{K_{gi}K_{\text{inv}}}(10^{\frac{T_{f1}}{20}}f_1 - f_c) \quad \textbf{(28)}$$

By substituting $j\omega_c$ for *s* in (7):

$$G_{PR}(j\omega_c) = K_P + \frac{2K_r\omega_{PRc}(j\omega_c)}{(j\omega_c)^2 + 2\omega_{PRc}(j\omega_c) + \omega_1^2} \quad \textbf{(29)}$$

As $(j\omega_c)^2 + 2\omega_{PRc}(j\omega_c)$ is far greater than ω_1^2, so the term ω_1^2 can be ignored and $G_{PR}(s)$ will be:

$$G_{PR}(s) = K_P + \frac{2K_r\omega_{PRc}}{s} \quad \textbf{(30)}$$

Assuming desired phase margin for the system to be PM, it can be inferred that:

$$\pi + \angle T(j\omega_c) = PM \quad \textbf{(31)}$$

Using (8) together with (28) and (29), K_r can be expressed as:

$$K_r = \frac{\left(\frac{L_1+L_2}{L_2C}\right) - 2\pi L_1 f_c^2 - K_{AD}K_{inv}f_c\tan(PM)}{K_{AD}K_{inv}f_c + \left(\left(\frac{L_1+L_2}{L_2C}\right) - 2\pi L_1 f_c^2\right)\tan(PM)} \cdot \frac{\pi f_c K_P}{w_{PRc}} \quad \textbf{(32)}$$

4.2.3 Capacitor Current Feedback Coefficient (K_{AD})

By substituting (24) and (28) in (31), K_{AD} is calculated as:

$$K_{AD} = \frac{(L_1+L_2)/L_2C - 2\pi L_1 f_c^2}{K_{inv}f_c} \times \frac{\pi f_c^2 - (10^{\frac{T_{f1}}{20}}f_1 - f_c)w_{PRc}\tan(PM)}{(10^{\frac{T_{f1}}{20}}f_1 - f_c)w_{PRc} + \pi f_c^2\tan(PM)} \quad \textbf{(33)}$$

The gain margin (GM) of the system at resonance frequency is calculated as following:

$$GM = -20\log\left|T(j\omega_r)\right| \quad \textbf{(34)}$$

Substituting $s = j\omega_r$ into (6) it's inferred that:

$$\left|G_{PR}(j\omega_r)\right| = \left|K_P + \frac{2K_r\omega_{PRc}(j\omega_r)}{(j\omega_r)^2 + 2\omega_{PRc}(j\omega_r) + \omega_1^2}\right| \quad \textbf{(35)}$$

As the denominator of the part, which contains K_r is far greater than the numerator part, this part can be ignored and (35) can be rewritten:

$$\left|G_{PR}(j\omega_r)\right| = K_P \quad \textbf{(36)}$$

Substituting (24) and (36) into (8) in $s = j\omega_r$, $T(j\omega_r)$ will be:

$$T(j\omega_r) = \frac{A}{B} = \frac{2\pi f_c(L_1+L_2)}{-(\omega_r)^2(L_2CK_{AD}K_{inv}) - j\omega_r(L_1L_2C\omega_r^2 + (L_1+L_2))} \quad \textbf{(37)}$$

$$\begin{cases} \left|A\right| = 2\pi f_c(L_1+L_2) \\ \left|B\right| = \dfrac{L_1+L_2}{L_1}\sqrt{(K_{AD}K_{inv})^2 + 4\omega_r^2L_1^2} \end{cases} \quad \textbf{(38)}$$

As $(K_{AD}.K_{inv})^2$ is far greater than $4\omega_r^2L_1^2$, the latter term can be ignored, so $T(j\omega_r)$ can be simplified to (39).

$$\left|T(j\omega_r)\right| = \frac{\left|A\right|}{\left|B\right|} = \frac{2\pi f_c L_1}{K_{AD}K_{inv}} \quad \textbf{(39)}$$

Considering (34) and (39), the minimum value of K_{AD} is expressed by (40):

$$K_{AD} = 10^{\frac{GM}{20}} \cdot \frac{2\pi f_c L_1}{K_{inv}} \quad \textbf{(40)}$$

4.2.4 Design Considerations

The magnitude of the open loop Transfer function at fundamental frequency, T_{f1}, is the starting point for controller parameter design. As mentioned in (18), T_{f1} should be greater than 40 dB. In this paper T_{f1} is supposed to be 45 dB.

After calculating K_P and defining T_{f1}, the next step is to calculate minimum resonant gain K_r by equation (28). Then the upper boundary of K_{AD} is obtained using (33). The lower boundary of K_{AD} depends on GM and cut-off frequency rather than intrinsic parameters of the system. By applying (40) and supposing the $GM = 5dB$ at resonance frequency, the minimum value of K_{AD} is obtained. After all, when the range of K_{AD} is defined, and the suitable value of K_{AD} is chosen, the upper boundary of K_r is calculated using (32). It should be noted that, by decreasing the value of K_{AD} the phase margin of the open loop system increases. To choose a suitable value for K_r, it should be taken into account that greater K_r leads to smaller GM.

5. Simulation Results

In this section, PV arrays are set as shown in Table 2. The LCL filter parameters are considered as Table 3. As the switching frequency is 10 kHz, the resonance frequency of the filter should be within the range of $f_{sw}/4$ to $f_{sw}/2$. The resonance frequency of LCL filter is 2516 Hz. To fulfil appropriate design and suitable performance of the grid connected LCL single-phase Trans-Z-source inverter, f_c is chosen a value lower than $f_{sw}/10$ [41]. Therefore, the cut-off frequency is set

to be 630 Hz. Using (24) K_P becomes 0.7265. By employing (28) the lower boundary of 11 is calculated for K_r. The upper boundary for the active damping coefficient using (33) is obtained as 0.3. Equation (40) gives the lower boundary of 0.041 for K_{AD}. K_{AD} is chosen to be 0.045 to achieve sufficient phase margin for the system. After definition of K_{AD}, the upper limit of K_r is calculated using the defined value of K_{AD} and (32), so K_r is in the range of 11 to 130. Considering suitable phase margin and gain margin, K_r is set to be 60 (about half of the maximum limit).

Fig. 7 shows the open loop bode diagram of the system. As can be seen, using designed parameters leads to a phase margin of 61.3 degrees and gain margin of 5.3 dB.

Table 2. Parameters of the solar panel at 25° C and solar irradiance of 1000 W/m^2

Parameter	Value
I_{mp}	30.44 A
V_{mp}	78.9 V
P_{max}	3075 W
I_{sc}	32.84 A
V_{oc}	98.7 V
N_s	3
N_P	5

Table 3. System parameters

Grid Voltage (RMS)	110 V
Grid frequency	60 Hz
Switching frequency	10 kHz
filter capacitance (C)	2200 µF
Transformer turn ratio (n)	2
Inverter side inductance (L_1)	1 mH
Filter capacitance	20 µF
Grid side inductance (L_2)	0.25 mH

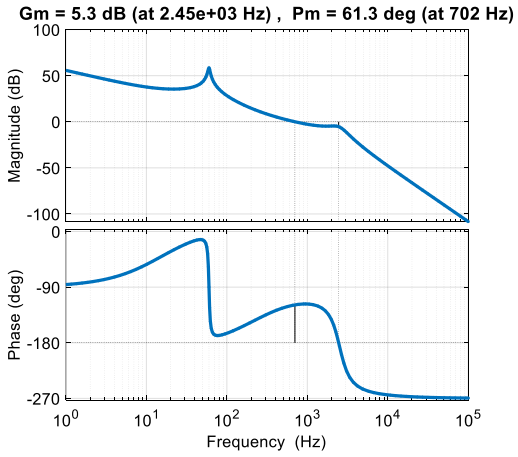

Fig. 7. Open loop bode diagram of the system

A comparison between the system with and without active damping scheme is illustrated in Fig. 8. Sharp rise of frequency response magnitude, due to LCL filter resonance can be seen around resonance frequency. As is shown, this sharp rise is completely softened using active damping. In Fig. 9 at t=0.4 s active damping is disabled and the grid current control will not work.

As depicted in Fig. 10 the MPPT method applied in this system has 91% efficiency obtaining 2770W of the nominal power (3075W) of PV arrays.

One of the two main goals of the control system is to inject power to the grid fulfilling grid standards. As shown in Fig. 11 a sinusoidal current with frequency of 60 Hz is injected to the grid and Fig. 12 confirms the unity power factor of the injected power as there is zero phase shift between grid voltage and grid current. Fig. 13 shows that THD of the injected grid current is 1.24%, which is a considerably low value.

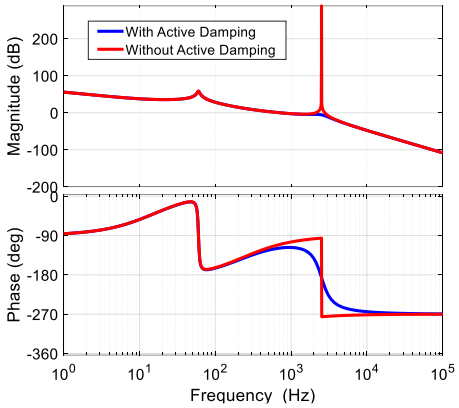

Fig. 8. Open loop bode diagram of the system of the system with and without active damping

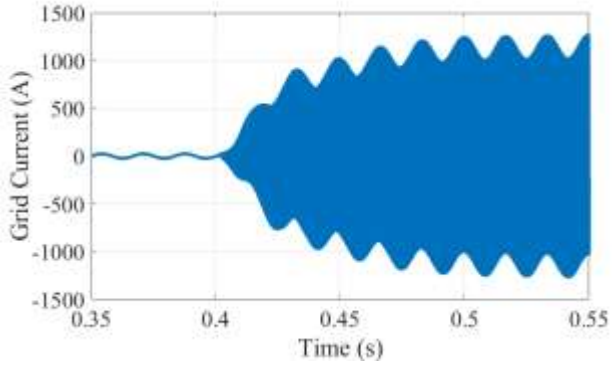

Fig. 9. Grid Current (the Active damping is disabled at t=0.4 s)

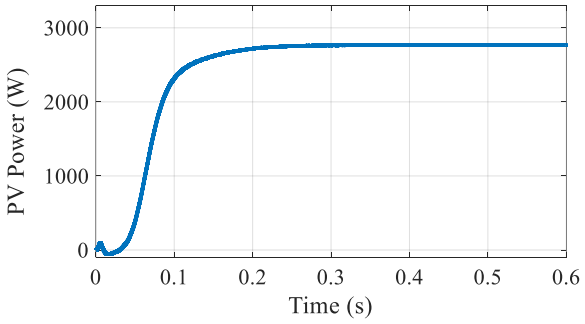

Fig. 10. PV power of the system with 91% efficiency

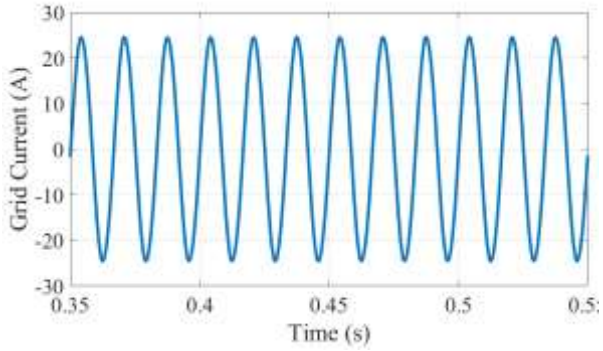

Fig. 11. Grid Current

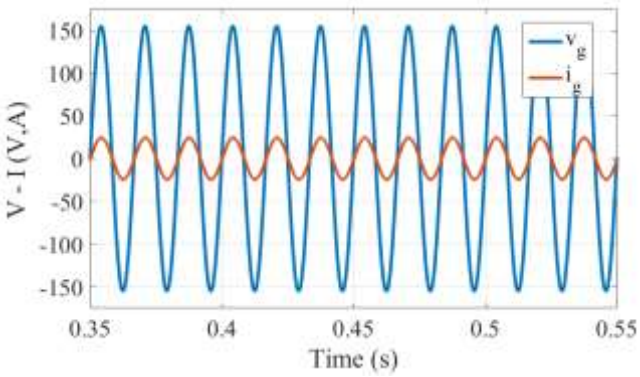

Fig. 12. Grid voltage and grid current

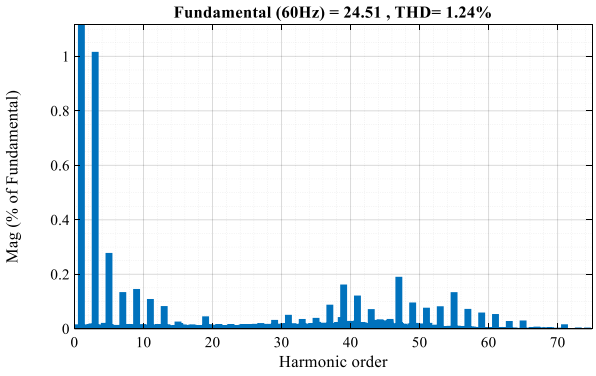

Fig. 13. Grid current THD

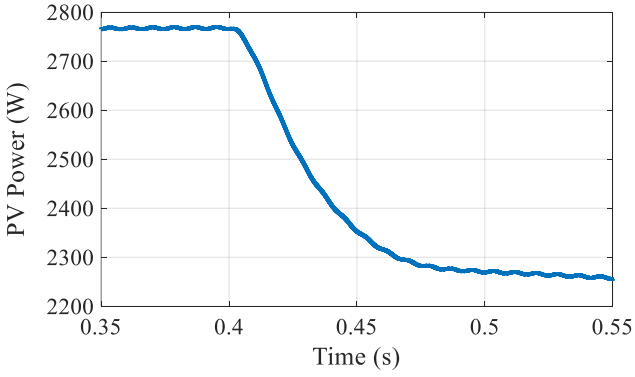

Fig. 14. PV power of the system exposed to temperature change from 25ºC to 45ºC at t=0.4 s

PV panels are exposed to weather condition changes, so the control system should maintain system stability during temperature changes and irradiance changes. In Fig. 14 the temperature is risen from 25 ºC to 45ºC at t=0.4 s. Fig. 15 shows that the control scheme can maintain system stability during temperature change at t=0.4 s.

Fig. 16 depicts the obtained PV power during irradiance change from 1000 W/m^2 to 850 W/m^2. The control system can keep the system in stable mode as shown in Fig. 17 in which the grid is controlled in the new condition caused by irradiance change at t=0.4 s. Therefore, it can be concluded that in both cases, the control system performs well and the system is stable against temperature and irradiance change.

The voltage stress of the Trans-Z-Source inverter switches, which are shown in Fig. 18, are a suitable value and the switches are not under high voltage stress. The Trans-Z-Source capacitor voltage is an important part of the control method. As pointed out in Fig. 19 the capacitor voltage ripple is acceptable which leads to satisfying performance of the grid side current control.

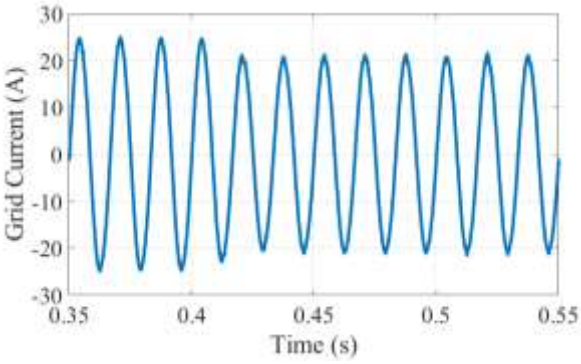

Fig. 15. Grid current exposed to temperature change from 25ºC to 45ºC at t=0.4 s

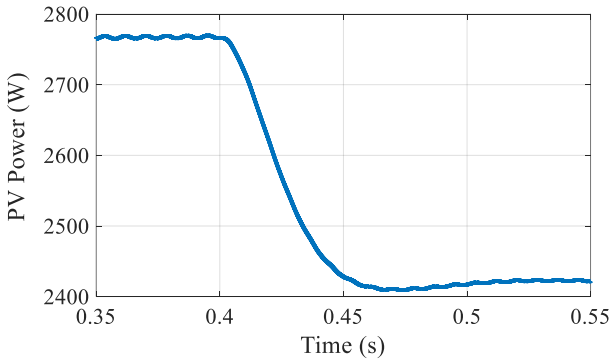

Fig. 16. PV power of the system exposed to irradiance change from 1000 W/m^2 to 850 W/m^2 at t=0.4 s

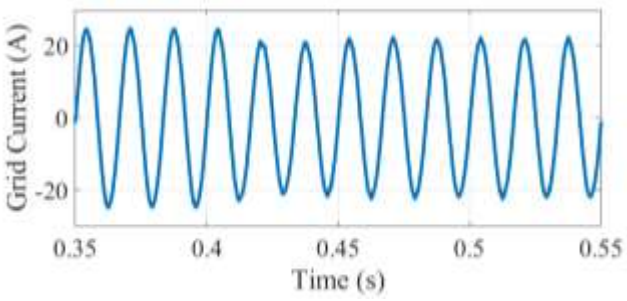

Fig. 17. Grid current exposed to irradiance change from 1000 W/m^2 to

850 W/m^2 at t=0.4 s

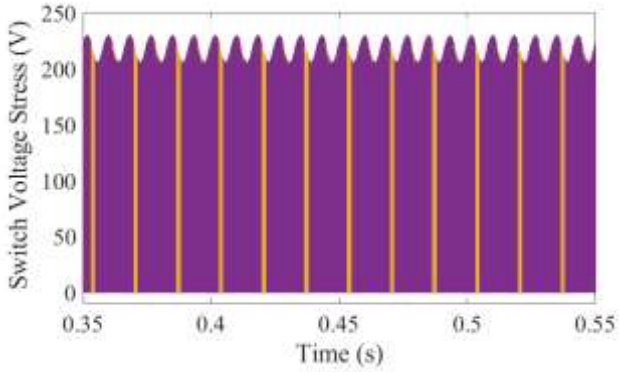

Fig. 18. Voltage stress of the inverter switches

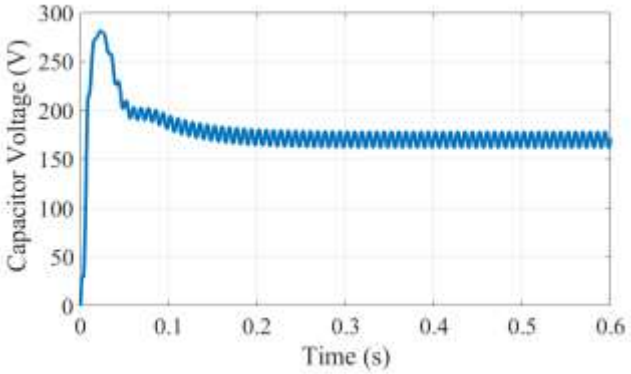

Fig. 19. DC link capacitor voltage

As Distributed, Power Generation (DPG) systems may be exposed to weak grid, it is important for the system to maintain its stability during grid voltage fluctuations. In the following four scenarios, the grid voltage amplitude changes. Voltage sag is the common case, so three cases in which the grid voltage drops by 0.1 p.u. (Fig. 20), 0.2 p.u. (Fig. 21) and 0.3 p.u. (Fig. 22) respectively, have been considered and in all cases the voltage variation starts at t=0.4 s and ends at t=0.55 s. As grid voltage swell is rare in weak grids, a case where 0.05 p.u. voltage swell is also considered which is depicted in Fig. 23. The THD of the injected current during grid voltage variation has been stated in the captions of figures.

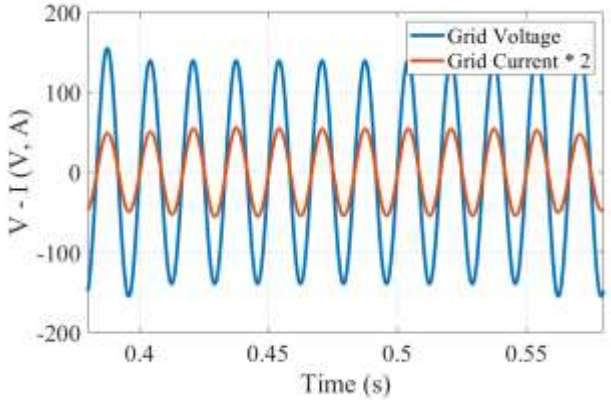

Fig. 20. Grid Voltage Sag by 0.1 p.u. at t=0.4 s to t=0.55 s (THDi=1.24%)

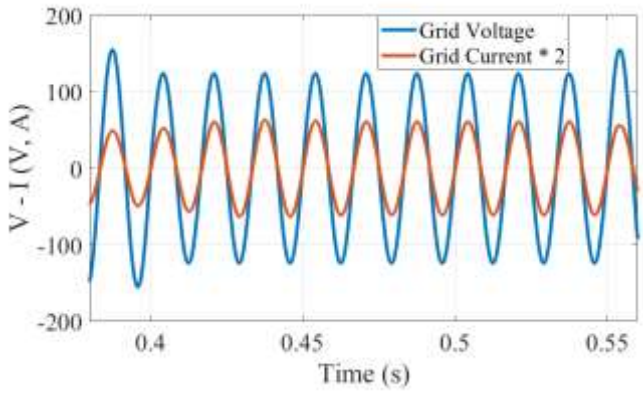

Fig. 21. Grid Voltage Sag by 0.2 at t=0.4 s to t=0.55 s (THDi =1.54%)

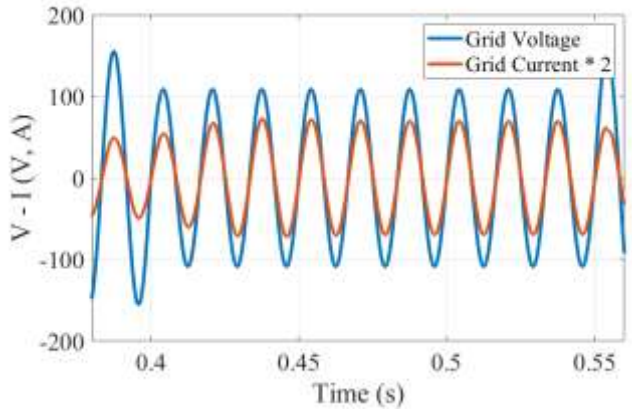

Fig. 22. Grid Voltage Sag 0.7 at t=0.4 s to t=0.55 s (THDi =2.08%)

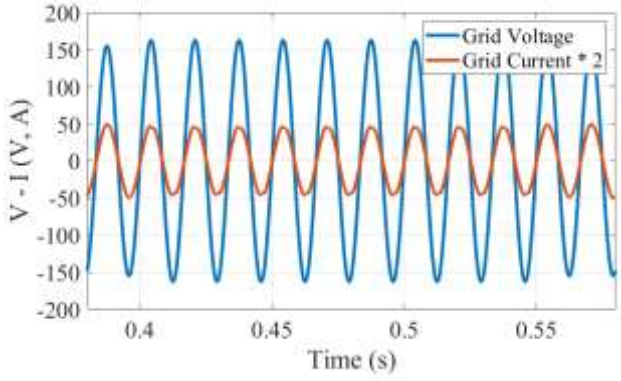

Fig. 23. Grid Voltage Swell 1.05 at t=0.4 s to t=0.55 s (THDi =2.97%)

In the following two figures, the injected current control of the system has been investigated under grid side inductance change. In the first case which is shown in Fig. 24 the grid side inductance value is doubled between t=0.4 s and t=0.5s and as depicted in Fig. 25, the second one shows the injected current to the grid, while the grid side inductance is half of its primary value. In both cases, the system maintains its stability and the control part performs well against variation of grid side inductance.

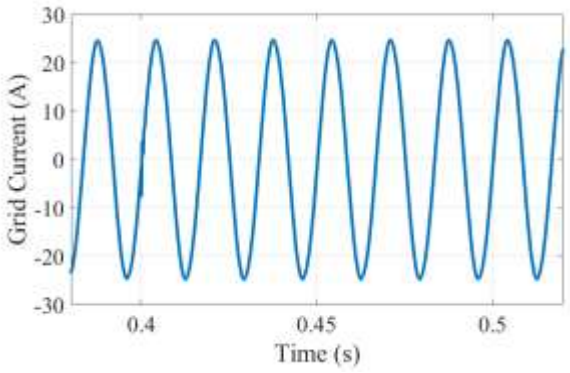

Fig. 24. Grid Side Inductance is doubled at t=0.4 s to t=0.5 s (THDi=1.19)

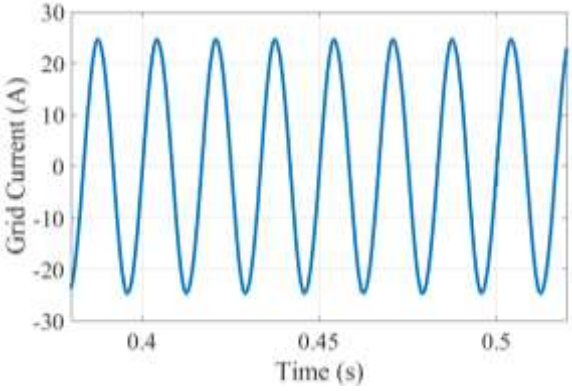

Fig. 25. Grid Side Inductance is halved at t=0.4 s to t=0.5 s (THDi=1.43)

6. Comparison with Similar Work Simulation Results

A similar structure has been proposed in [11] in which a Trans-Z-Source based inverter PV is connected to the grid by L filter. In the mentioned work, the control system samples grid current and capacitor voltage. To ensure the unity power factor, a PLL block is used to synchronize injected current with the grid voltage. The MPPT method which is used in the current paper is the same as [11]. The difference is on the output filter and the control technique. In this work, a LCL filter is applied and an active damping along with carefully tuned PR controller leads to improved control of the injected power to the grid. The grid current THD in a pure sinusoidal grid voltage in [11] is 2.90%, while the proposed control system in the current paper has achieved grid current THD of 1.24%. As summarized in table 4, by a LCL filter and a systematically tuned PR controller, adopting active damping of capacitor current lead to better performance of the injected power control to the grid.

To suppress undesired harmonics in injected current to the grid, different approaches have been proposed. In [43] an active damping method based on linear active disturbance rejection control is proposed which THD_i of 1.16% is resulted. In [44] a design procedure for capacitor current feedback active damping of voltage oriented PI control of grid-tied converters has been proposed which leads to grid current THD of 1%. The analysis of grid-connected inverters using LCL filter with capacitor voltage feedforward active damping has been carried out in [45] in which THD_i of 1% is achieved.

In the current work PV panel utilizing MPPT technique has been applied in the input of the system while in the aforementioned references a battery is the input. Tracking the maximum power point leads to ripple of the output voltage of the Trans-Z-Source converter, therefore as shown in table 5 the THD of the injected current may be slightly more than systems with batteries as input source.

7. Conclusion

Due to development of grid-tied PV based inverters as Distributed Power Generators, the control of injected power to the grid becomes more important. In this work a control scheme for a PV based Trans-Z-Source inverter which is connected to the grid through LCL filter is proposed and also a systematic method for designing the controller parameters and active damping factor is also provided. The control method performs well on MPPT, the injected power meets the grid codes, and the grid current THD is considerably reduced compared with similar works. Simulation results have been performed during weather change condition to analyze the performance of the system in such circumstances.

References

[1] Chowdhury, A., et al. A Complete Comparison of the two Maximum Power Point Tracking Technique (MPPT) for Photovoltaic systems. in 2018 4th International Conference on Electrical Energy Systems (ICEES). 2018.

[2] Singh, N. and S.K. Jain. "Single phase Z-source inverter for photovoltaic system", *in 7th India International Conference on Power Electronics (IICPE)*, 2016.

[3] Peng, F.Z., "Z-source inverter", *IEEE Transactions on industry applications*, 39, (2003): 504-510.

[4] Shen, M., et al., "Constant boost control of the Z-source inverter to minimize current ripple and voltage stress", *IEEE transactions on industry applications*, 42, (2006): 770-778.

[5] Peng, F.Z., M. Shen, and Z. Qian, "Maximum boost control of the Z-source inverter", *IEEE Transactions on power electronics*, 20, (2005): 833-838.

[6] Qian, W., F.Z. Peng, and H. Cha, "Trans-Z-source inverters", *IEEE transactions on power electronics*, 26, (2011): 3453-3463.

[7] Siwakoti, Y.P., et al. "Y-source impedance network", in *Twenty-Ninth Annual IEEE Applied Power Electronics Conference and Exposition (APEC)*, (2014).

[8] Siwakoti, Y.P., F. Blaabjerg, and P.C. Loh, "Quasi-Y-source boost dc–dc converter", *IEEE Transactions on Power Electronics*, 30, (2015): 6514-6519.

[9] Li, Y., et al. "Quasi-Z-source inverter for photovoltaic power generation systems", in *Twenty-Fourth Annual IEEE Applied Power Electronics Conference and Exposition*, (APEC), (2009).

[10] Vinnikov, D., et al., "High-performance quasi-Z-source series resonant DC–DC converter for photovoltaic module-level power electronics applications", *IEEE Transactions on Power Electronics*, 32, (2017): 3634-3650.

[11] Rajabi, A., M. Simab, and J. Aghaei, "Design of a Power-Conditioning System for Trans-Z-Source Inverter to Connect Photovoltaic Arrays to Single-Phase Household Electrical Grid", *Iranian Journal of Science and Technology, Transactions of Electrical Engineering*, 42, (2018): 393-402.

[12] Committee, I.S.C., "IEEE Standard for Interconnecting Distributed Resources with Electric Power Systems", IEEE Std1547-2003, 2009.

[13] Huang, M., et al. "Step by step design of a high order power filter for three-phase three-wire grid-connected inverter in renewable energy system", in *4th IEEE International Symposium on Power Electronics for Distributed Generation Systems (PEDG)*, 2013.

[14] Lu, M., et al., "Benchmarking of Stability and Robustness Against Grid Impedance Variation forLCL-Filtered Grid-Interfacing Inverters", *IEEE Transactions on Power Electronics*, 33, (2018): 9033-9046.

[15] Ruan, X., et al., "Control techniques for LCL-type grid-connected inverters", *Springer*, (2018).
[16] Bahrani B., M. Vasiladiotis and A. Rufer, "High-Order Vector Control of Grid-Connected Voltage-Source Inverters with LCL-Filters", *IEEE Transactions on Industrial Electronics*, 61, (2014): 2767-2775.
[17] Wang X., F. Blaabjerg, P. C. Loh, "Virtual RC Damping of LCL-Filtered Voltage Source Inverters with Extended Selective Harmonic Compensation", *IEEE Transactions on Power Electronics*, 30, (2010): 4726-4737.
[18] Wang X., X. F. Blaabjerg, P. C. Loh, "Grid-Current-Feedback Active Damping for LCL Resonance in Grid-Connected Voltage Source Inverters", *IEEE Transactions on Power Electronics*, 3, (2016): 213-223.
[19] Pan D., X. Ruan, C. Bao, W. Li and X. Wang, "Capacitor-Current-Feedback Active Damping With Reduced Computation Delay for Improving Robustness of LCL-Type Grid-Connected Inverter", *IEEE Transactions on Power Electronics*, 29, (2014): 3414-3427.
[20] Pan D., X. Ruan, C. Bao, W. Li, X. Wang, "Optimized Controller Design for LCL-Type Grid-Connected Inverter to Achieve High Robustness against Grid-Impedance Variation", *IEEE Transactions on Industrial Electronics*, 62, (2015): 1537-1547.
[21] Rasekh N., M.M. Rahimian, M. Hosseinpour, A. Dejamkhooy, A. Akbarimajd, "A Step by Step Design Procedure of PR controller and Capacitor Current Feedback Active Damping for a LCL-Type Grid-tied T-Type Inverter", in *10th International Power Electronics, Drive Systems and Technologies Conference (PEDSTC)*, (2019): 4483-4491.
[22] Yang D., X. Ruan and H. Wu, "A Real-Time Computation Method with Dual Sampling Modes to Improve the Current Control Performances of the LCL-Type Grid-Connected Inverter", *IEEE Transactions on Industrial Electronics*, 62, (2015): 4563-4572.
[23] Bao, C., et al., "Step-by-step controller design for LCL-type grid-connected inverter with capacitor–current-feedback active-damping", *IEEE Transactions on Power Electronics*, 29, (2014): 1239-1253.
[24] Li X., X. Wu, Y. Geng, X. Yuan, C. Xia, and X. Zhang, "Wide Damping Region for LCL-Type Grid-Connected Inverter with an Improved Capacitor-Current-Feedback Method", *IEEE Transactions on Power Electronics*, 30, (2015): 5247-5259.
[25] Kukkola J. and M. Hinkkanen, "State Observer for Grid-Voltage Sensorless Control of a Inverter Equipped With an LCL Filter: Direct Discrete-Time Design", *IEEE Transactions on Industry Applications*, 52, (2016): 3133-3145.
[26] Dannehl J., F. W. Fuchs, S. Hansen, and P. B. Thogersen, "Investigation of active damping approaches for PI-based current control of grid-connected pulse width modulation inverters with LCL filters", *IEEE Transactions on Industry Applications*, 46, (2010): 1509-1517.
[27] Alzola R. P., M. Liserre, F. Blaabjerg, R. Sebastian, J. Dannehl, and F. W. Fuchs, "Systematic design of the lead-lag network method for active damping in LCL-filter based three-phase inverters", *IEEE Transactions on Industrial Informatics*, 10, (2014): 43-52.
[28] Xin Z., P. C. Loh, X. Wang, F. Blaabjerg, and Y. Tang, "Highly Accurate Derivatives for LCL-Filtered Grid Inverter with Capacitor Voltage Active Damping", *IEEE Transactions on Power Electronics*, 31, (2016): 3612-3625.
[29] Komurcugil H., N. Altin, S. Ozdemir and I. Sefa, "Lyapunov-Function and Proportional-Resonant-Based Control Strategy for Single-PhaseGrid-Connected VSI With LCL Filter", *IEEE Transactions on Industrial Electronics*, 63, (2016): 2838-2849.
[30] Huang M., X. Wang, P. C. Loh, and F. Blaabjerg, "Active Damping of LLCL-Filter Resonance Based on LC-Trap Voltage or Current Feedback", *IEEE Transactions on Power Electronics*, 31, (2016): 2337-2346.
[31] Wu, W., L. Yuan, H. Yuanbin, H. Chung, M. Liserre, and F. Blaabjerg, "Damping methods for resonances caused by LCL-filter-based current-controlled grid-tied power inverters: An overview", *IEEE Transactions on Industrial Electronics*, 64, (2017): 7402-7413.
[32] Hosseinpour M., Dejamkhooy A., "Control and power sharing among parallel three-phase three-wire and three-phase four-wire inverters in the presence of unbalanced and harmonic loads", *IEEJ Transactions on Electrical and Electronic Engineering*, 13, (2018): 1027-1033.
[33] Liu, J., L. Zhou, and M. Molinas, "Damping region extension for digitally controlled LCL-type grid-connected inverter with capacitor-current feedback", *IET Power Electronics*, 11, (2018): 1974-1982.
[34] Zhang, N., H. Tang, and C. Yao, "A systematic method for designing a PR controller and active damping of the LCL filter for single-phase grid-connected PV inverters", *Energies*, 7, (2014): 3934-3954.
[35] Sangwongwanich, A., Y. Yang, and F. Blaabjerg, "A sensorless power reserve control strategy for two-stage grid-connected PV systems", *IEEE Transactions on Power Electronics*, 32, (2017): 8559-8569.
[36] Judewicz, M.G., et al., "Inverter-Side Current Control of Grid-Connected Voltage Source Inverters With LCL Filter Based on Generalized Predictive Control", *IEEE Journal of Emerging and Selected Topics in Power Electronics*, 6, (2018): 1732-1743.
[37] Anderson, J. and F.Z. Peng. "Four quasi-Z-source inverters", in *Power Electronics Specialists Conference (PESC)*, 2008.
[38] Yang, S., et al., "Current-fed quasi-Z-source inverter with voltage buck–boost and regeneration capability", *IEEE Transactions on Industry Applications*, 47, (2011): 882-892.
[39] Sera, D., et al. "Improved MPPT algorithms for rapidly changing environmental conditions". in *12th International Power Electronics and Motion Control Conference (EPE-PEMC)*, 2006.
[40] Wu, W., et al. "DSP-based multiple peak power tracking for expandable power system" in *Eighteenth Annual IEEE Applied Power Electronics Conference and Exposition (APEC'03)*, 2003.
[41] Bao, C., et al. "Design of injected grid current regulator and capacitor-current-feedback active-damping for LCL-type grid-connected inverter", in *Energy Conversion Congress and Exposition (ECCE)*, 2012.
[42] Akagi, H., "Active harmonic filters". *Proceedings of the IEEE*, 93(12), (2005): 2128-2141.
[43] Benrabah, A., X. Dianguo, and Z. Gao. "Active Disturbance Rejection Control ofLCL-Filtered Grid-Connected Inverter Using Padé Approximation", *IEEE Transactions on Industry Applications*, 54, (2018): 6179-6189.
[44] Rodriguez-Diaz, E., F. D. Freijedo, J. Vasquez, and J. M. Guerrero. "Analysis and Comparison of Notch Filter and Capacitor Voltage Feedforward Active Damping Techniques for LCL Grid-Connected Converters", *IEEE Transactions on Power Electronics*, 34, (2019): 3958 - 3972.
[45] Saïd-Romdhane, M. Ben, M. Wissem Naouar, I. Slama-Belkhodja, and E. Monmasson. "Robust active damping methods for LCL filter-based grid-connected converters", *IEEE Transactions on Power Electronics*, 32, (2017): 6739-6750.